Neurochemistry International 61 (2012) 1102–1113

Contents lists available at SciVerse ScienceDirect

Neurochemistry International

journal homepage: www.elsevier.com/locate/nci

Synergistic anti-cancer mechanisms of curcumin and paclitaxel for growth inhibition of human brain tumor stem cells and LN18 and U138MG cells

Md. Motarab Hossain [a], Naren L. Banik [b], Swapan K. Ray [a,*]

[a] Department of Pathology, Microbiology, and Immunology, University of South Carolina School of Medicine, Columbia, SC, United States
[b] Department of Neurosciences, Medical University of South Carolina, Charleston, SC, United States

ARTICLE INFO

Article history:
Received 17 February 2012
Received in revised form 1 August 2012
Accepted 6 August 2012
Available online 13 August 2012

Keywords:
Angiogenesis
Apoptosis
Brain tumor stem cells
Glioblastoma
Network formation

ABSTRACT

Glioblastoma, the deadliest brain tumor in humans, responds poorly to conventional chemotherapeutic agents because of existence of highly chemoresistant human brain tumor stem cells (HBTSC). An effective therapeutic strategy is urgently needed to target HBTSC as well as other glioblastoma cells. We explored synergistic efficacy of a low dose of curcumin (CCM) and a low dose of paclitaxel (PTX) in HBTSC and human glioblastoma LN18 (p53 mutant and PTEN proficient) and U138MG (p53 mutant and PTEN mutant) cells. The highest expression of the cancer stem cell markers aldehyde dehydrogenase 1 (ALDH1) and CD133 occurred in HBTSC when compared with LN18 and U138MG cells. Combination of 20 μM CCM and 10 nM PTX worked synergistically and more effectively than either drug alone in decreasing viability in all cells. Combination of CCM and PTX was highly effective in inducing both morphological and biochemical features of apoptosis. Apoptosis required activation of caspase-8, cleavage of Bid to tBid, increase in Bax:Bcl-2 ratio, and mitochondrial release of cytochrome *c*, Smac, and apoptosis-inducing factor (AIF). Phosphorylation of Bcl-2 following combination therapy appeared to promote Bax homodimerization and mitochondrial release of pro-apoptotic factors into the cytosol. Increases in activities of cysteine proteases confirmed the completion of apoptotic process. Combination therapy inhibited invasion of cells, reduced expression of survival and proliferation factors and also angiogenic factors, and prevented HBTSC, LN18, and U138MG cells from promoting network formation. Collectively, the combination of CCM and PTX worked as a promising therapy for controlling the growth of HBTSC and other glioblastoma cells.

1. Introduction

Glioblastoma is the most malignant primary brain tumor, which hardly responds to conventional chemotherapies (Porter et al., 2010). Patients with glioblastoma have the poorest prognosis with survival time less than a year. Due to heterogeneous nature, glioblastoma cells are highly resistant to conventional chemotherapies. Recently, it has been reported that conventional chemotherapy and radiation therapy target mostly the CD133-negative population, evading the CD133-positive population (Bao et al., 2006). These CD133-positive cells are cancer stem cells that occupy a minor part of tumor mass even then they play an essential role in relapsing and reforming the tumor repeatedly after the therapy (Reya et al., 2001). Human brain tumor stem cells (HBTSC) can exist in glioblastoma to continue tumor formation and angiogenesis, and contribute to chemoresistance (Bleau et al., 2009). Conventional therapies are capable of removing only the better differentiating cells, sparing the HBTSC that can continue tumor recurrence (Zhou et al., 2009).

Tumor tissues comprise various types of cells including resting stem cells, proliferating transit-amplifying cells, terminally differentiating cells, and apoptotic cells (Sell, 2006). The transit-amplifying cells in tumor tissues do not mature into terminally differentiating cells and continue to proliferate without destine to die (maturation arrest). Due to maturation arrest properties of tumor cells, their populations continue to increase in tumor tissues while cell populations in normal tissues remain reasonably constant (Sell, 2006). The actively proliferating transit-amplifying cells can be killed by conventional radiation and chemotherapy but cancer stem cells restore transit-amplifying population (Gilbert and Ross, 2009). Obviously, HBTSC population is a potential therapeutic target in glioblastoma treatment (Das et al., 2008b). The CD133 is a widely known cancer stem cell marker (Shi et al., 2011), but recently aldehyde dehydrogenase 1 (ALDH1) is used as the most important brain tumor stem cell marker (Rasper et al., 2010).

Curcumin (CCM), a phytochemical from turmeric (*Curcuma longa*), has shown anti-cancer properties in both *in vitro* and *in vivo* models (Epstein et al., 2010). Besides, CCM suppresses

* Corresponding author. Tel.: +1 803 216 3420; fax: +1 803 216 3428.
E-mail address: swapan.ray@uscmed.sc.edu (S.K. Ray).

0197-0186/$ - see front matter © 2012 Elsevier Ltd. All rights reserved.
http://dx.doi.org/10.1016/j.neuint.2012.08.002

carcinogenesis in skin, forestomach, mammary, colon, and liver in different *in vivo* animal models (Epstein et al., 2010). CCM also affects proliferation through cell cycle arrest and cytotoxicity against cancer cells such as HL-60, K562, MCF-7, T98G, and HeLa cells for induction of apoptosis (Karunagaran et al., 2005; Karmakar et al., 2006). CCM alone suppresses anti-apoptotic signals and induces apoptosis via extrinsic and intrinsic caspase cascades in human glioblastoma cells (Karmakar et al., 2007).

Paclitaxel (PTX), which belongs to taxane family, is a highly effective anti-cancer drug that stoichiometrically binds to microtubule and stabilizes microtubule structure (Xiao et al., 2006). Thus, mitotic spindle dynamics is suppressed leading to cell cycle arrest at G2/M phase and induction of apoptosis (McGrogan et al., 2008). The anti-cancer efficacy of PTX is well established in treatment of patients with lung, ovarian, bladder, breast, and head-and-neck cancers (Rowinsky et al., 1993; Crown and O'Leary, 2000). PTX also inhibits tumor-angiogenesis through down-regulation of vascular endothelial growth factor (VEGF) production (Toiyama et al., 2009) and matrix metalloproteinase (MMP) expression (Stearns and Wang, 1992). PTX also controls growth of glioblastoma cells through down-regulation of epidermal growth factor receptor (EGFR), nuclear factor-kappa B (NF-κB), phospho-Akt (p-Akt), and multi-drug resistance (MDR) marker (Choudhury et al., 2011).

Our present study demonstrated that combination of CCM and PTX worked synergistically and controlled growth of HBTSC as well as of LN18 and U138MG cells by upregulating pro-apoptotic molecules, increasing Bax:Bcl-2 ratio, phosphorylating Bcl-2, and down-regulating the molecules involved in cell survival and angiogenesis.

2. Materials and methods

2.1. Cell culture and conditions

We obtained human brain tumor stem cells (HBTSC) from Celprogen (San Pedro, CA, USA). Human glioblastoma LN18 and U138MG cell lines were purchased from the American Type Culture Collection (Manassas, VA, USA). We have selected two different glioblastoma cell lines because of their different status of the tumor suppressor phosphatase and tensin homolog located on chromosome 10 (PTEN), which is wild type in LN18 cell line and mutated and not expressed in U138MG cell line. We propagated HBTSC in Ham's F12 but LN18 and U138MG in DMEM, both media supplemented with 10% fetal bovine serum (FBS) (Atlanta Biological, Atlanta, GA, USA) and 1% penicillin–streptomycin, in a fully humidified incubator containing 5% CO_2 at 37 °C. CCM (Sigma, St. Louis, MO, USA) was dissolved in dimethyl sulfoxide (DMSO) to make 10 mM small aliquots and store at −20 °C until use. PTX (7.03 mM) was procured from Bristol-Myers Squibb (Princeton, NJ, USA) and diluted to 1 mM solution with DMSO, protected from light, and stored at −20 °C until use. CCM and PTX were further diluted in cell culture media containing 1% FBS before use.

2.2. Antibodies

The antibodies against ALDH1, CD31, and cytochrome *c* were purchased from BD Biosciences (San Jose, CA, USA); antibody against β-actin (clone AC-15) was from Sigma (St. Louis, MO, USA), and antibodies against p-Akt (Thr 308), b-FGF, calpain, caspase-3, caspase-8, ICAD, MMP-2, MMP-9, PARP, p65 NF-κB, Bax, Bcl-2, Bid, survivin, hTERT, CD133, VEGF, and cytochrome *c* oxidase 4 (COX4) were purchased from Santa Cruz Biotechnology (Santa Cruz, CA, USA). Antibody against TATA binding protein (TBP) was obtained from abcam (Cambridge, MA, USA). Alkaline horseradish peroxidase (HRP) conjugated anti-rabbit and anti-mouse secondary IgG antibodies were purchased from Biomeda (Foster City, CA, USA) and alkaline HRP conjugated anti-goat secondary IgG antibody was obtained from Santa Cruz Biotechnology (Santa Cruz, CA, USA).

2.3. Immunofluorescence microscopy

Immunofluorescence microscopy was performed according to a previously described method (Rasper et al., 2010). Briefly, cells were grown on poly-D-lysine chamber slides (BD Biosciences, San Jose, CA, USA) at 37 °C in presence of 5% CO_2 for 24 h and washed in phosphate-buffered saline (PBS), pH 7.4, (without $Ca^{2+}$and Mg^{2+}) followed by fixation with 4% formaldehyde in PBS, pH 7.4, for 30 min at room temperature. Cells were incubated for 10 min with 0.25% Triton X-100 in PBS to make them permeable and washed again with PBS. Non-specific binding were blocked by incubation with 3% bovine serum albumin (BSA) in PBS for 10 min followed by overnight incubation with the primary IgG antibody against ALDH1 (BD Biosciences, San Jose, CA, USA) in 1% BSA at 4 °C. The primary antibody was removed, washed with PBS, and stained with fluorescein isothiocyanate (FITC) conjugated anti-mouse secondary IgG antibody (Jackson Immunoresearch, West Grove, PA) for 1 h at room temperature and washed again with PBS. The nuclear stain 4′-6-diamidino-2-phenylindole (DAPI) was used to stain the nuclei of the cells. DAPI forms complex with double-stranded DNA, showing a blue fluorescence. Cells were incubated with 300 nM DAPI (Invitrogen, Eugene, OR, USA) for 5 min and washed four times with PBS before mounting the cells with Dabco 33-LV (Sigma, St. Louis, MO, USA). Images were captured under the Zeiss LSM 510 META laser scanning confocal microscopy Zeiss, Germany) and analyzed by the Zeiss LSM image software.

2.4. Determination of cell viability using the 3-(4,5-dimethylthiazol-2-yl)-2,5-diphenyltetrazolium bromide (MTT) assay

The effects of different concentrations of CCM, PTX, and their combinations on the viability of HBTSC, LN18, and U138MG cells were determined by the MTT assay (Purnanam and Boustany, 1999). Briefly, cells were grown in 100 μl medium containing 2% FBS in 96-well plates at 37 °C. After 24 h, we replaced old medium with fresh medium containing 1% FBS with or without drugs and incubated for another 24 h at 37 °C. After treatments, media were discarded and cells were washed with PBS and incubated with MTT (0.2 mg/ml) in 100 μl fresh medium for 2 h. Then, 2-propanol (200 μl) was added to dissolve MTT formazan crystals and absorbance was measured at 570 nm in a plate reader (BioTek, Winooski, VT, USA). Cell viability was calculated as percentage of viable cells in total population. Compusyn software (ComboSyn, Paramus, NJ, USA) was used for determining the combination index (CI) values of the data from MTT assay. Conventionally, combination of drugs with CI > 1, CI = 1, and CI < 1 is showing antagonism, additive effect, and synergism, respectively.

2.5. In situ Wright staining for detection of morphological features of apoptosis

Cells were grown in 2 ml medium containing 2% FBS in 6-well dishes at 37 °C. After 24 h, we replaced old medium with fresh medium containing 1% FBS with or without drugs and incubated for another 24 h at 37 °C. After the treatments, cells were washed with PBS and then fixed and subjected to the Wright staining according to the manufacturer's instructions (Fisher Scientific, Kalamazoo, MI, USA). After the *in situ* Wright staining, cells were dried and morphological features of apoptotic cells were observed under the light microscope as we recently reported (Choudhury et al., 2010).

2.6. Annexin V staining and flow cytometry for detection of a biochemical feature of apoptosis

Cells were grown in 2 ml medium containing 2% FBS in 6-well dishes at 37 °C. After 24 h, we replaced old medium with fresh medium containing 1% FBS with or without drugs and incubated for another 24 h at 37 °C. After treatments, cells were washed twice with 10 ml PBS, stained with Annexin V-FITC/propidium iodide (PI), processed as per manufacturer's instructions (BD Biosciences, San Diego, CA, USA), and then analyzed on an Epics XL-MCL Flow Cytometer (Beckman Coulter, Fullerton, CA, USA). Both PI and Annexin V negative cells (quadrant B3) were considered as normal, PI negative and Annexin V positive cells were considered as early apoptotic (quadrant B4), cells that were both PI and Annexin V positive (quadrant B2) were considered as late necrotic, and cells that were PI positive and Annexin V negative were considered as mechanically injured (quadrant B1).

2.7. Protein extraction

Cells were grown in 150-mm dishes in medium containing 10% FBS at 37 °C. After 24 h, we replaced old medium with fresh medium containing 1% FBS with or without drugs and incubated for another 24 h at 37 °C. After treatments, cells were scraped, collected, and centrifuged to obtain the pellet. The cell pellets were washed twice in 20 ml ice-cold PBS. Each cell pellet was suspended in 400 μl ice-cold homogenization solution (50 mM Tris–HCl, pH 7.4, 320 mM sucrose, 0.1 mM phenylmethylsulfonyl fluoride, and 1 mM EDTA), transferred to 1.5-ml Eppendorf tube, and subjected to sonication gently in micro-ultrasonic cell disruptor (Kontes, Vineland, NJ, USA). The cell lysates were centrifuged at 12,000 rpm for 10 min at 4 °C and the supernatants were collected. Mitochondria and cytosolic fractions were separated according to the supplier's instructions (Pierce Biotechnology, Rockford, IL, USA) to analyze the mitochondrial release of cytochrome *c*. The protein concentrations were measured using the Coomassie plus protein assay reagents (Pierce Biotechnology, Rockford, IL, USA).

2.8. Isolation of cytosolic and nuclear fractionations

After trypsinization, cells were pelleted at 1000 rpm for 4 min, washed with PBS, and pelleted again at 1000 rpm for 4 min. The pellet was suspended in 5 ml of ice-cold hypotonic buffer A (10 mM Hepes, pH 7.9, 1.5 mM $MgCl_2$, 10 mM KCl, and 0.5 mM DTT) and kept on ice for 5 min. The cells were broken using a pre-chilled dounce homogenizer (20 strokes with a tight pestle) to release nuclei in buffer and centrifuged at 228*g* for 5 min at 4 °C. Supernatant was collected and retained it as the cytosolic fraction. The pellet was suspended in 3 ml of buffer S1 (0.25 mM sucrose and 10 mM $MgCl_2$), layered over a 3 ml cushion of buffer S2 (0.88 mM sucrose and 0.5 mM $MgCl_2$), and centrifuged at 2800*g* (3500 rpm in Beckman GS-6 centrifuge using GH-3.8 rotor) for 10 min at 4 °C. We collected the pellet, suspended in RIPA buffer (50 mM Tris–HCl, pH 7.5, 150 mM NaCl, 1% NP-40, and 0.5% deoxycholate), and retained it as nuclear fraction.

2.9. Western blotting

After the treatments, protein samples extracted from the cells were resolved by sodium dodecyl sulfate–polyacrylamide gel electrophoresis (SDS–PAGE) for Western blotting. Briefly, the protein samples (10 μg) were mixed with Laemmli buffer, heated in boiling water for 5 min, loaded onto the precast 4–20% SDS–polyacrylamide gradient gels (Bio-Rad Laboratories, Hercules, CA, USA), resolved by SDS–PAGE, and electroblotted to the polyvinylidene fluoride (PVDF) membranes (Millipore, Bedford, MA, USA). The non-specific binding sites in the membrane were blocked with 5% non-fat dry milk for 1 h at room temperature. The membranes were then incubated overnight at 4 °C for shaking on a rocker with appropriate dilution of primary IgG antibody followed by three times washing in a washing buffer (20 mM Tris–HCl, pH 7.6, 137 mM NaCl, and 0.1% Tween 20). After washing, the membranes were incubated with appropriate alkaline horseradish peroxidase (HRP) conjugated secondary IgG antibody for 1 h followed by three times washing in the washing buffer. Specific protein bands were detected by incubation for 5 min at room temperature with Immun-Star™ HRP Lumino/Enhancer (Bio-Rad Laboratories, Hercules, CA, USA) and autoradiography with exposure to BIOMAX XAR films (Kodak, Rochester, NY, USA).

2.10. In vitro invasion assay

The effects of CCM and PTX alone and in combination on the invasive properties of HBTSC, LN18, and U138MG cells through a matrigel were determined by the *in vitro* invasion assay (George et al., 2010a). Briefly, *in vitro* invasion assay was carried out in 6-well transwell inserts of polycarbonate filter with 8.0 μm pore size (Corning Life Sciences, Manassas, VA, USA). The transwell inserts were coated with the matrigel (BD Biosciences, San Diego, CA, USA) of final concentration of 1.0 mg/ml in an ice-cold serum-free medium and allowed to dry at 37 °C for 4 h. The cells were treated with CCM and PTX alone and in combination for 24 h. After treatments, cells were trypsinized, washed twice with serum-free medium, and 500 μl of cell suspension (1×10^5 cells) from each sample was added to each Transwell insert in triplicate. Cells were then incubated at 37 °C in presence of 5% CO_2 for 48 h and membranes were collected and stained with the DIFF QUICK STAIN Kit (IMEB, San Marcos, CA, USA). The cells that migrated to the undersurface of the membrane were observed by light microscopy, photographed, and counted in 10 randomly selected microscopic fields.

2.11. In vitro angiogenesis assay

In vitro angiogenesis assay was performed to evaluate the effects of CCM and PTX alone or in combination on network formation of human microvascular endothelial (HME) cells (Cascade Biologics, Portland, OR, USA) in co-culture. HBTSC, LN18, and U138MG cells (1×10^5) were seeded separately into 2-well chamber slides. After 24 h, cells were treated with CCM, PTX, or their combination in serum-free medium. Cells were incubated for 24 h and then co-cultured with 1×10^5 HME cells in a 50:50 mixture of serum-free medium and HME medium (Medium 131, Cascade Biologics, Portland, OR, USA). The co-cultures were further incubated at 37 °C in presence of 5% CO_2 for 72 h and then cells were fixed with 95% ice-cold ethanol and treated with Von Willebrand factor (VWF) antibody (Santa Cruz Biotechnology, Santa Cruz, CA, USA). After washings, the slides were further treated with biotinylated secondary antibody for 30 min, washed twice with PBS, and then incubated with HRP labeled streptavidin for 30 min. Cells were stained with the HRP substrate according to the ImmunoCruz™ Staining System instructions (Santa Cruz Biotechnology, Santa Cruz, CA, USA). The cells were viewed under the light microscope and photographed. The numbers of network formation were quantified using the Image-Pro Discovery software (Media Cybernetics, Silver Spring, MD, USA).

2.12. Statistical analysis

Results obtained from different experiments were analyzed using Minitab® 15 statistical software (Minitab, State College, PA, USA) and compared using one-way analysis of variance (ANOVA) with Fisher's post hoc test. All data were presented as

mean ± standard deviation (SD) of separate experiments ($n \geqslant 3$). Difference between control and a single or combination treatment was considered to be significant at a p value less than 0.05.

3. Results

3.1. Identification of cancer stem cell markers

We examined the levels of expression of cancer stem cell markers, ALDH1 and CD133, in HBTSC, LN18, and U138MG cells (Fig. 1). Western blotting demonstrated that ALDH1 was highly expressed in HBTSC, moderately in LN18 cells, and slightly in U138MG cells (Fig. 1A). On the other hand, CD133 was moderately expressed in HBTSC and LN18 cells but slightly in U138MG cells. We further used immunofluorescence microscopy to confirm levels of expression of ALDH1 in HBTSC, LN18, and U138MG cells. We found that HBTSC was highly positive and LN18 was partially positive for ALDH1 while U138MG was negative (Fig. 1B). DAPI was used as the nuclear stain.

3.2. Combination of CCM and PTX acted synergistically for growth inhibition

We treated HBTSC, LN18, and U138MG cells with different concentrations of CCM (5, 10, and 20 μM) and PTX (5, 10, and 25 nM) alone and in their combinations for 24 h (Fig. 2). The MTT assay

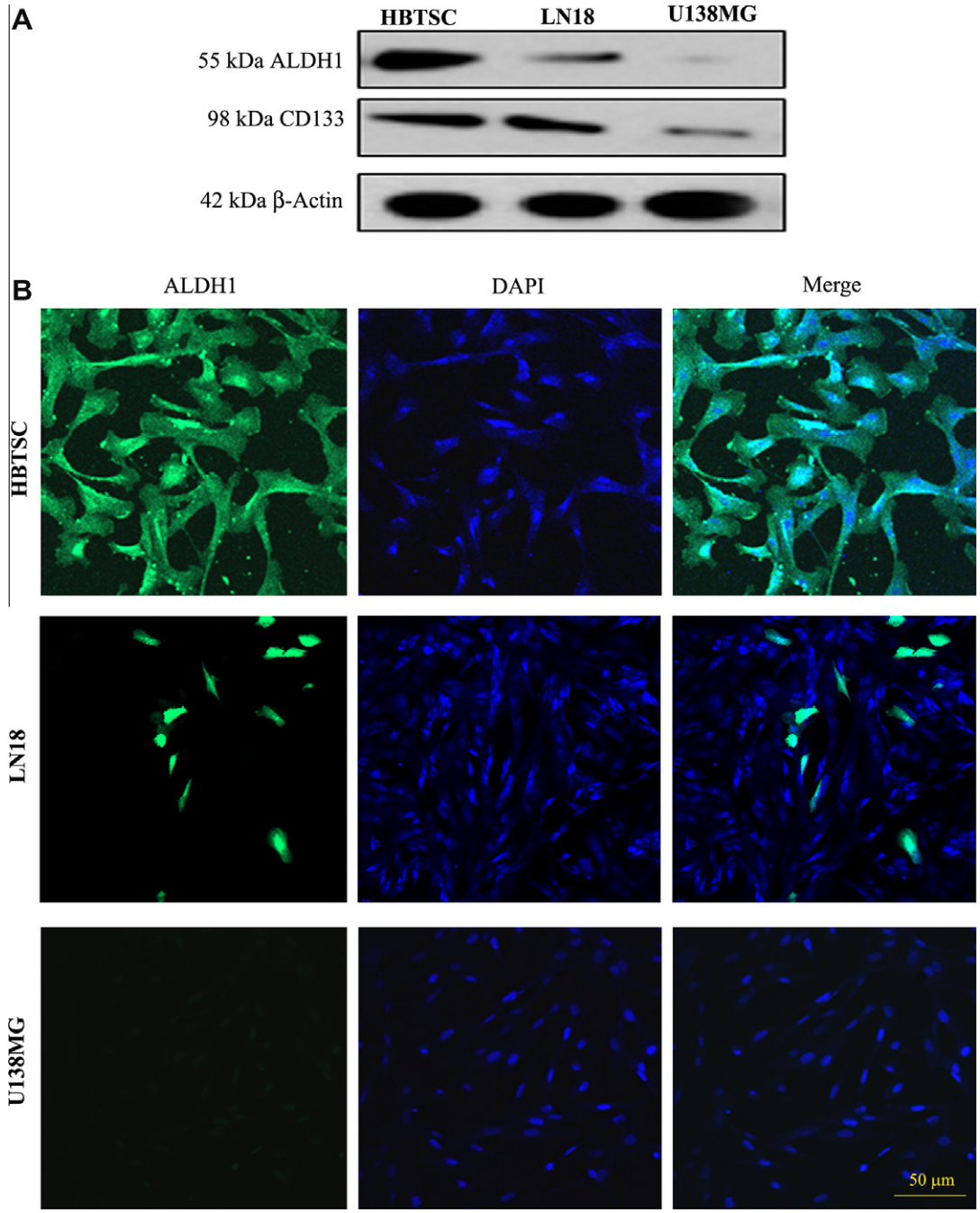

Fig. 1. Examination of cancer stem cell markers. (A) Representative Western blots to show the levels of the stem cell markers ALDH1 and CD133 in HBTSC, LN18, and U138MG cells. (B) Immunofluorescence staining showing expression of ALDH1 in HBTSC, LN18, and U138MG cells.

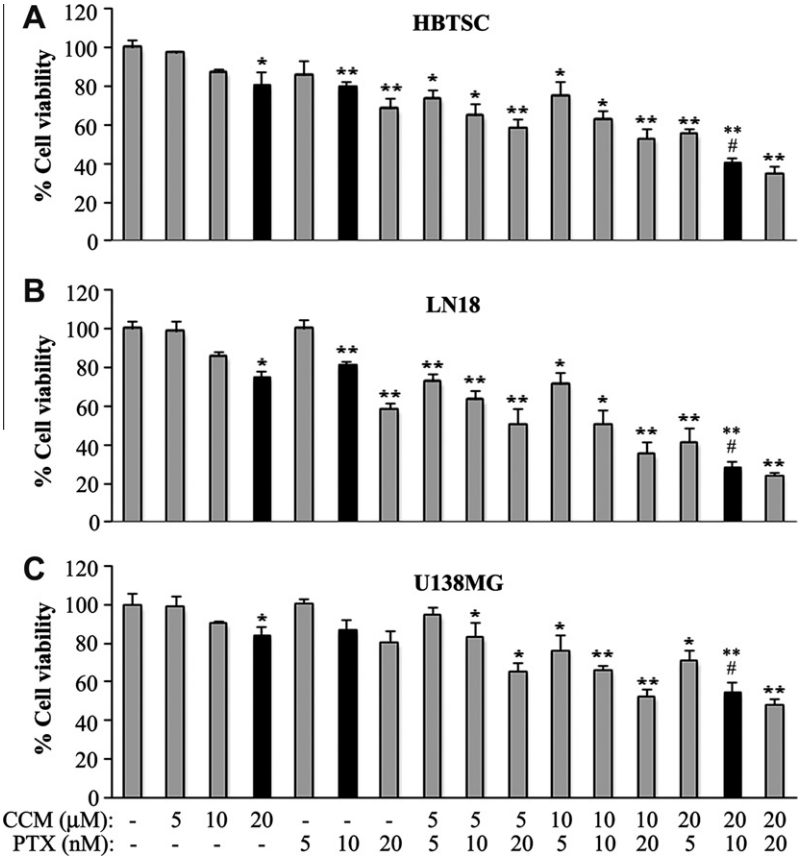

Fig. 2. Determination of residual cell viability. Amounts of residual cell viability of (A) HBTSC, (B) LN18, and (C) U138MG cells after treatments for 24 h with different concentrations of curcumin (CCM; 5, 10, or 20 μM), paclitaxel (PTX; 5, 10, or 20 nM) or their combinations. Mean values ($n = 3$) are shown ($^{*}p < 0.05$; $^{**}p < 0.01$; and $^{\#}p < 0.01$ where * or ** compared single treatment with CTL; # compared combination treatment with single treatment).

Table 1
Combination index (CI) of the drugs in HBTSC, LN18, and U138MG cells.

CCM (μM)	PTX (nM)	CI values		
		HBTSC	LN18	U138MG
5.0	5.0	0.52008	0.62561	1.44480
5.0	10.0	0.40145	0.68684	0.91033
5.0	20.0	0.40720	0.71747	0.33800
10.0	5.0	0.73859	0.7751	0.41205
10.0	10.0	0.38388	0.42150	0.23613
10.0	20.0	0.24189	0.30867	0.10347
20.0	5.0	0.14302	0.17247	0.36743
20.0	**10.0**	**0.02944**	**0.10330**	**0.08532**
20.0	20.0	0.02215	0.13168	0.06456

CI > 1 indicates antagonism, CI = 1 indicates additive effect, and CI < 1 indicates synergism. The lowest CI value (shown in bold number) indicates the best synergistic effect of the combination of two drugs for inhibition of cell viability and induction of apoptosis.

showed that CCM and PTX alone and in their combinations inhibited cell viability dose dependently. We analyzed the results from the MTT assay using the Compusyn software to determine the CI values of the combination of two drugs (Table 1). Although treatment of cells with 20 μM CCM or 10 nM PTX inhibited viability to some extent, their combination most effectively inhibited viability of HBTSC, LN18, and U138MG cells (Fig. 2). Combination of 20 μM CCM and 10 nM PTX worked synergistically in all these cells (Table 1). Notably, lower CI value indicated higher synergistic effect of the combination of drugs. Although we found a lower CI value of combination of 20 μM CCM and 20 nM PTX than combination of 20 μM CCM and 10 nM PTX (Table 1), we did not want to continue with the combination of 20 μM CCM and 20 nM PTX that showed too much cytotoxicity (necrotic cells) as we found in the *in situ* Wright staining (data not shown). Therefore, we selected 20 μM CCM and 10 nM PTX for single or combination treatments in all subsequent experiments.

3.3. Combination of CCM and PTX induced morphological features of apoptosis

We examined the effects of CCM and PTX alone and in combination on cells leading to induction of morphological features of apoptosis, including blebbing, shrinkage of cell volume, nuclear fragmentation, chromatin condensation and fragmentation, and membrane attached apoptotic bodies (Fig. 3). These characteristic morphological changes appeared after PTX treatment and highly increased with the combination of CCM and PTX (Fig. 3A). PTX alone induced apoptosis in HBTSC as well as in LN18 and U138MG cells but combination of CCM of PTX most significantly increased the amounts of apoptosis in all these cells (Fig. 3B).

3.4. Combination of CCM and PTX induced an early biochemical feature of apoptosis

We further confirmed induction of apoptosis by the Annexin V-FITC/PI staining and flow cytometry that showed the externalization of a membrane phospholipid, an early biochemical feature of apoptosis, in HBTSC, LN18, and U138MG cells after the treatments (Fig. 4). Representative data (Fig. 4A) indicated that Annexin V positive cells, the apoptotic populations, appeared in B4 quadrant after treatment with CCM or PTX. Interestingly, combination

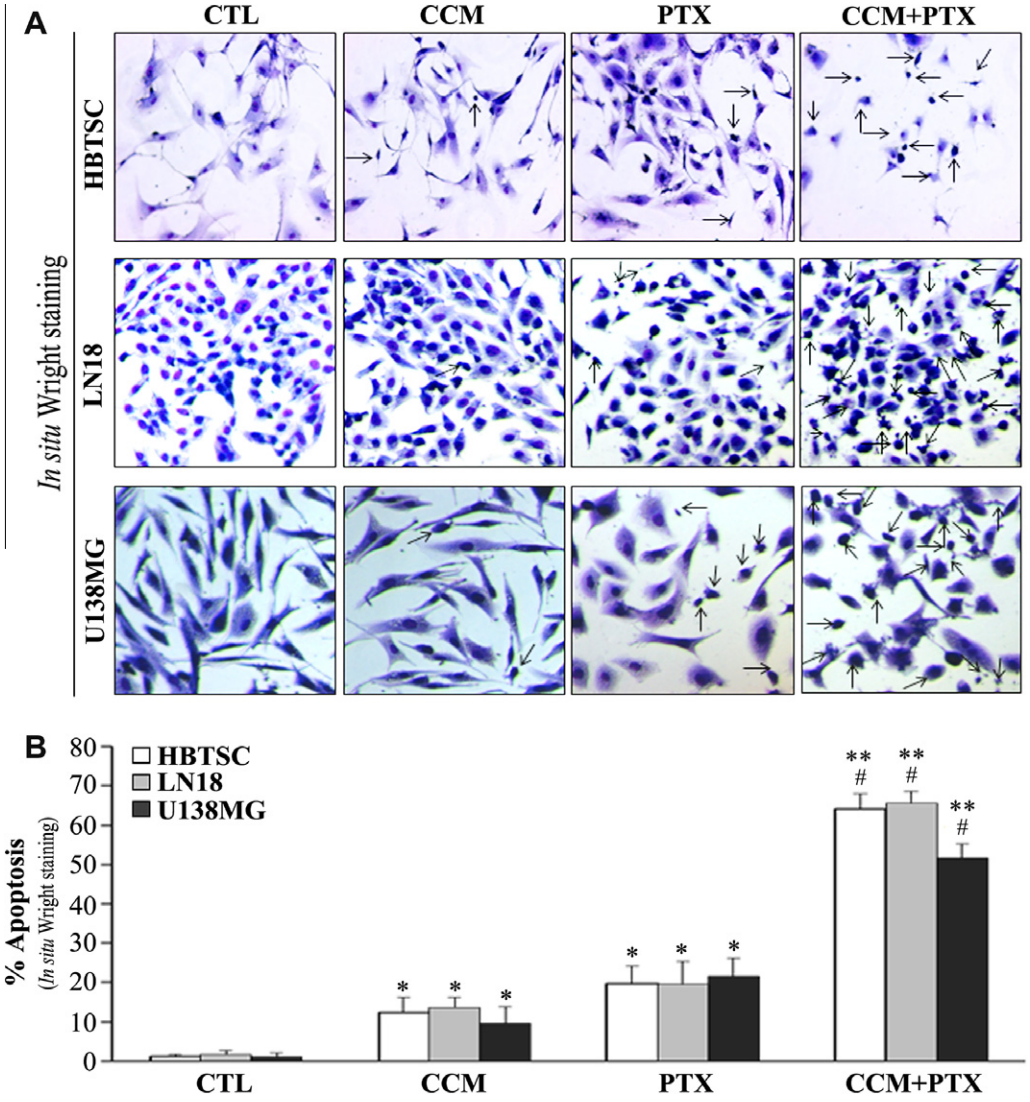

Fig. 3. Determination of morphological features of apoptosis. Treatments (24 h): control (CTL), 20 μM CCM, 10 nM PTX, and 20 μM CCM + 10 nM PTX. (A) *In situ* Wright staining for morphological features of apoptotic cells (arrows). (B) Bar diagrams showing percentage of apoptosis based on Wright staining. Mean values ($n = 3$) compared with CTL are shown ($^{*}p < 0.05$; $^{**}p < 0.01$). Significant difference between a combination treatment and a single treatment is also indicated ($\#p < 0.01$).

of CCM and PTX significantly increased the apoptotic populations in HBTSC, LN18, and U138MG cells (Fig. 4B). Notably, our Annexin V-FITC/PI staining followed by flow cytometric analyses showed that cell death was not related to cells expressing lower level of ALDH1. Because amounts of cell death were comparable in HBTSC, LN18, and U138MG cells after the treatment with the single agent or the two agents together.

3.5. Combination of CCM and PTX activated extrinsic and intrinsic caspase cascades

We employed Western blotting to examine the changes in expression of the molecules involved in activation of both extrinsic and intrinsic caspase cascades for apoptosis following treatments (Fig. 5). Almost uniform expression of β-actin was used as the cytosolic protein loading control (Fig. 5A). Combination therapy most impressively activated caspase-8, the classical player of extrinsic pathway, which cleaved Bid to tBid in all the cells. Combination therapy also highly increased expression of Bax (pro-apoptotic) and concomitantly reduced expression of Bcl-2 (anti-apoptotic) so as to favor apoptotic death via intrinsic pathway (Fig. 5B). We also examined expression of phosphorylated Bcl-2 (p-Bcl-2), the inactive form of Bcl-2, after the treatments and found that PTX induced expression of p-Bcl-2, which was further increased following combination therapy (Fig. 5B). Notably, p-Bcl-2 would not be able to heterodimerize with Bax to confer anti-apoptotic function.

We separated the cytosolic and mitochondrial fractions to examine the cytochrome *c* levels by Western blotting (Fig. 5C). We used uniform expression of COX4 as the mitochondrial protein loading control. Treatment of cells with combination of CCM and PTX most dramatically caused mitochondrial release of cytochrome *c* as well as of Smac/Diablo and AIF into the cytosol to promote the intrinsic pathway of apoptosis (Fig. 5C).

Next, we determined activation of the cysteine proteases, calpain and caspase-3, and their activities (Fig. 5D). Activation of both calpain and caspase-3 occurred in all cells after treatment with the combination CCM and PTX (Fig. 5D). We monitored calpain and caspase-3 activities in the formation of 145 kDa spectrin breakdown product (SBDP) and 120 kDa SBDP, respectively (Fig. 5D). We found that combination therapy most dramatically increased the levels of 145 kDa SBDP and 120 kDa SBDP in all cells (Fig. 5D). We further examined the proteolytic activity of

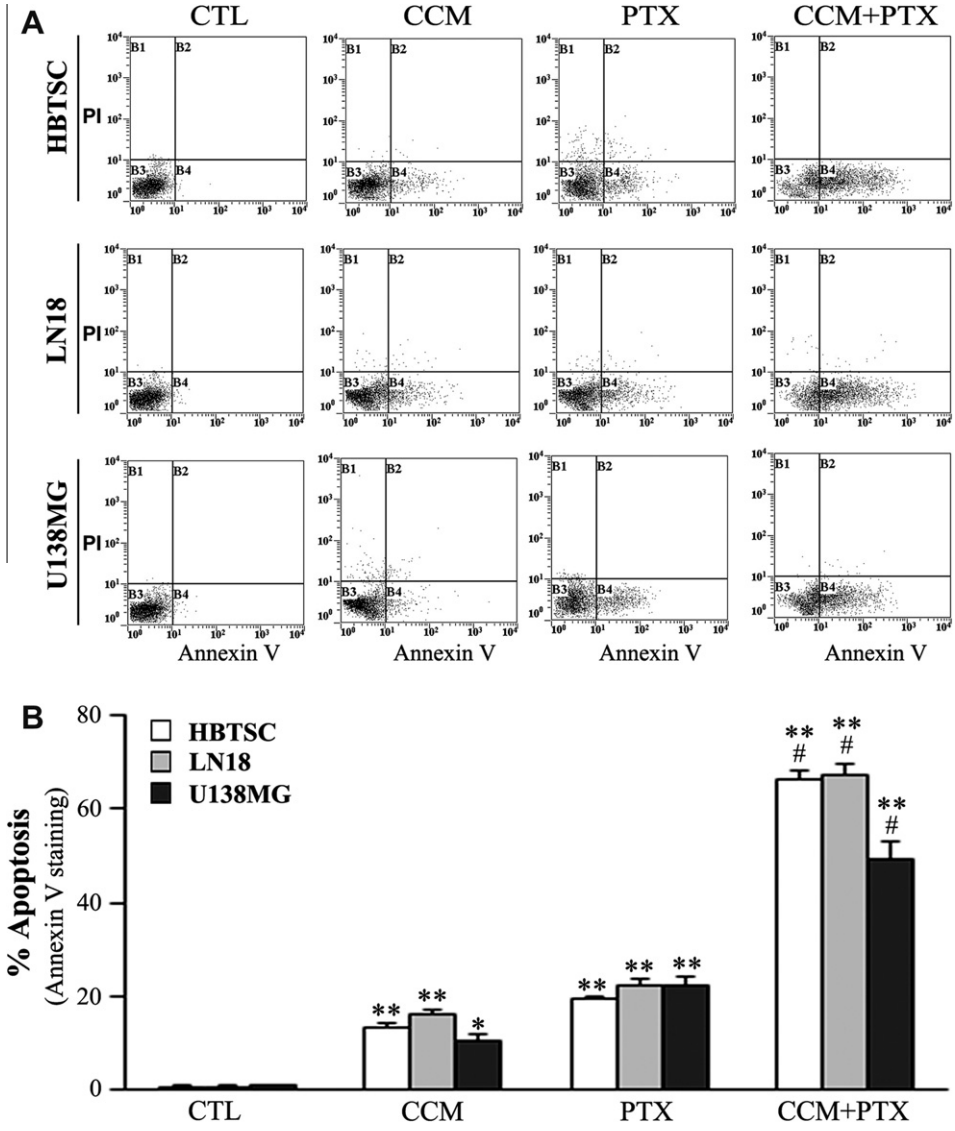

Fig. 4. Determination of the percentages apoptosis by Annexin V-FITC/PI staining and flow cytometric analysis. Treatments (24 h): control (CTL), 20 μM CCM, 10 nM PTX, and 20 μM CCM + 10 nM PTX. (A) Apoptotic cells (Annexin V-FITC positive and PI negative) are represented by dot plot in B4 quadrant (bottom right). (B) Bar diagrams showing percentage of apoptosis. Mean values ($n = 3$) are shown ($^{*}p < 0.05$; $^{**}p < 0.01$; and $^{\#}p < 0.01$ where * or ** compared single treatment with CTL; # compared combination treatment with single treatment).

caspase-3 in the fragmentation of the nuclear DNA repair enzyme poly(ADP-ribose) polymerase (PARP) and the cleavage of the inhibitor of caspase-3 activated DNase (ICAD) (Fig. 5D). Fragmentation of PARP and ICAD further confirmed an increase in caspase-3 activity for induction apoptosis.

3.6. Combination of CCM and PTX prevented cell invasion

We examined the effects of CCM or/and PTX on the cell invasion capability of cells by matrigel invasion assay (Fig. 6). Cells underneath the membrane that invaded through the matrigel on the polycarbonate membrane were stained and examined under the light microscope. Control HBTSC, LN18, and U138MG cells easily invaded through the matrigel and also there was little effect on cell invasion after treatment with CCM or PTX alone; however, there was a dramatic reduction in cell invasion through matrigel when cells were treated with combination of CCM and PTX (Fig. 6A). The percentages of cells invaded through the transwell membrane were presented in the bar graphs, which clearly showed that combination of CCM and PTX significantly reduced cell invasion (Fig. 6B).

3.7. Combination of CCM and PTX down-regulated molecules involved in cell survival, proliferation, invasion, and angiogenesis

We employed Western blotting to examine changes in expression of molecules involved in cell survival, proliferation, invasion, and angiogenesis after the treatments (Fig. 7). We separated the cytosolic and nuclear fractions to examine the levels of NF-κB by Western blotting after the treatments. We used uniform expression of β-actin as the cytosolic protein loading control and TATA binding protein (TBP) as the nuclear protein loading control. Treatment of cells with combination of CCM and PTX dramatically decreased levels of NF-κB in cytosolic fraction as well as in nuclear fraction (Fig. 7), indicating a possibility of ubiquitination and degradation of cytosolic NF-κB. Combination of CCM and PTX drastically down-regulated the molecules involved in cell survival (p-Akt and NF-κB), proliferation (survivin and hTERT), invasion

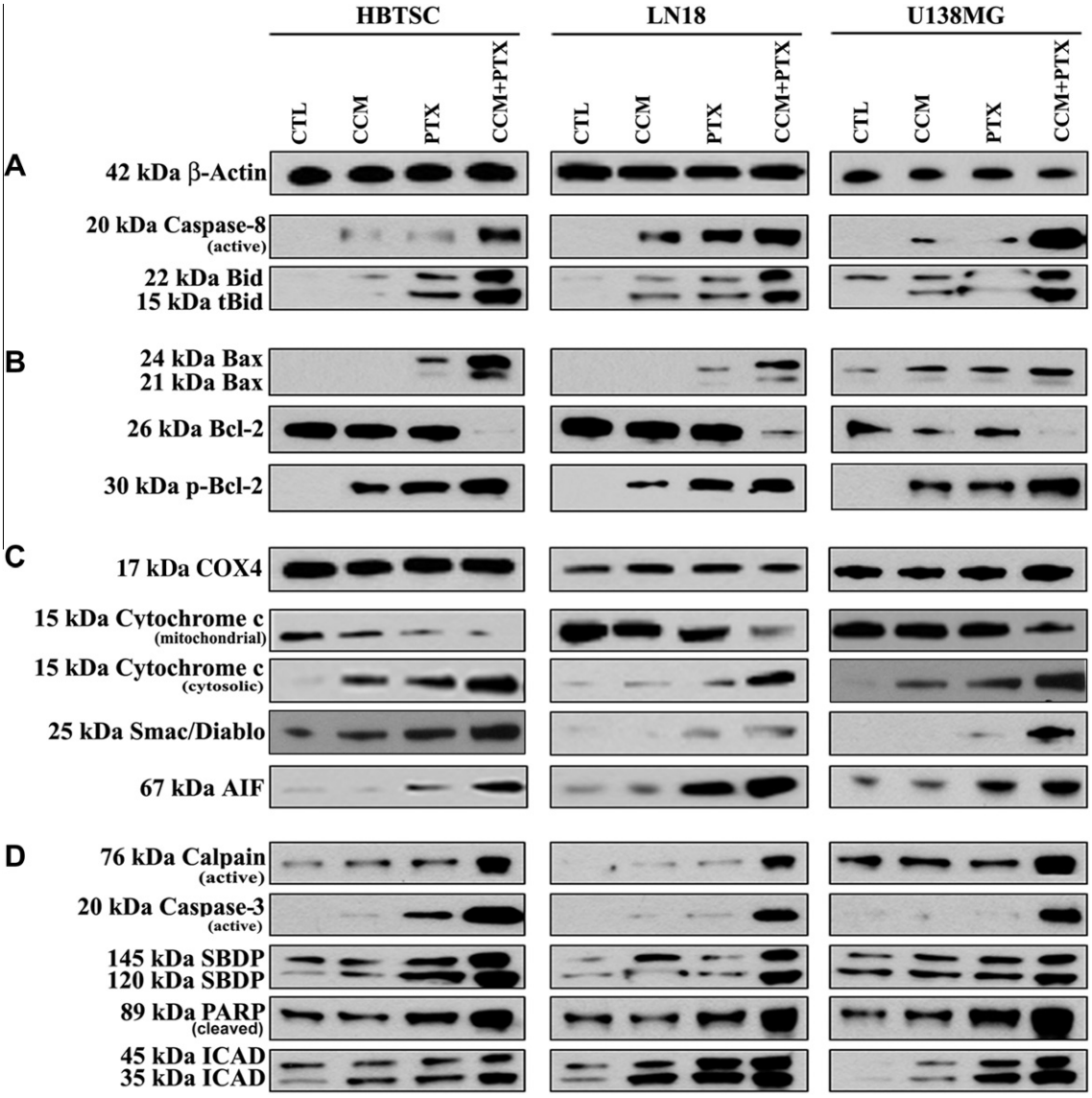

Fig. 5. Western blotting to examine molecules involved in induction of apoptosis. Treatments (24 h): control (CTL), 20 μM CCM, 10 nM PTX, and 20 μM CCM + 10 nM PTX. (A) Induction of extrinsic caspase pathway of apoptosis. (B) Expression of Bax and Bcl-2 and phosphorylation of Bcl-2 (p-Bcl-2). (C) Induction of intrinsic or mitochondrial pathway of apoptosis. (D) Activation of proteases and proteolytic activities. All experiments were repeated three times.

(MMP-2 and MMP-9), and angiogenesis (VEGF, b-FGF, and CD31) pathways.

3.8. Combination of CCM and PTX inhibited network formation

We examined the angiogenic network formation in co-culture of HME cells and HBTSC, LN18, or U138MG cells after the treatments (Fig. 8). Von Willebrand factor, a characteristic marker for endothelial cells, was used to identify the capillary-like network formation. We found that untreated HBTSC, LN18, and U138MG cells were quite supportive to HME cells for network formation (Fig. 8). But network formation was marginally reduced when co-cultured with HBTSC or glioblastoma cells treated with PTX alone; however, there was a drastic effect on the reduction in network formation when co-cultured with the cells treated with combination of CCM and PTX (Fig. 8A). Bar graphs clearly showed significant efficacy of combination therapy for inhibition of angiogenic network formation (Fig. 8B).

4. Discussion

Our goal in this study was to reveal the molecular mechanisms of synergistic action of CCM and PTX at low doses for growth inhibition of HBTSC, LN18, and U138MG cells. ALDH1 is used as a novel stem cell marker in solid tumors including lung cancer (Jiang et al., 2009), colorectal cancer (Huang et al., 2009) as well as glioblastoma LN18 cells (Rasper et al., 2010). We found expression of ALDH1 and CD133 most prominently in HBTSC and LN18 cells but slightly in U138MG cells. Combination of CCM and PTX inhibited growth of HBTSC, LN18, and U138MG cells via induction of extrinsic and intrinsic pathways of apoptosis and suppression of cell migration, survival and angiogenic factors, and capability of network formation. Our experiments showed that CCM and PTX at the low doses modulated different signaling pathways in different degrees but worked synergistically in a combination for controlling the growth of these cells. Our results for the first time established that combination of CCM and PTX could be used at

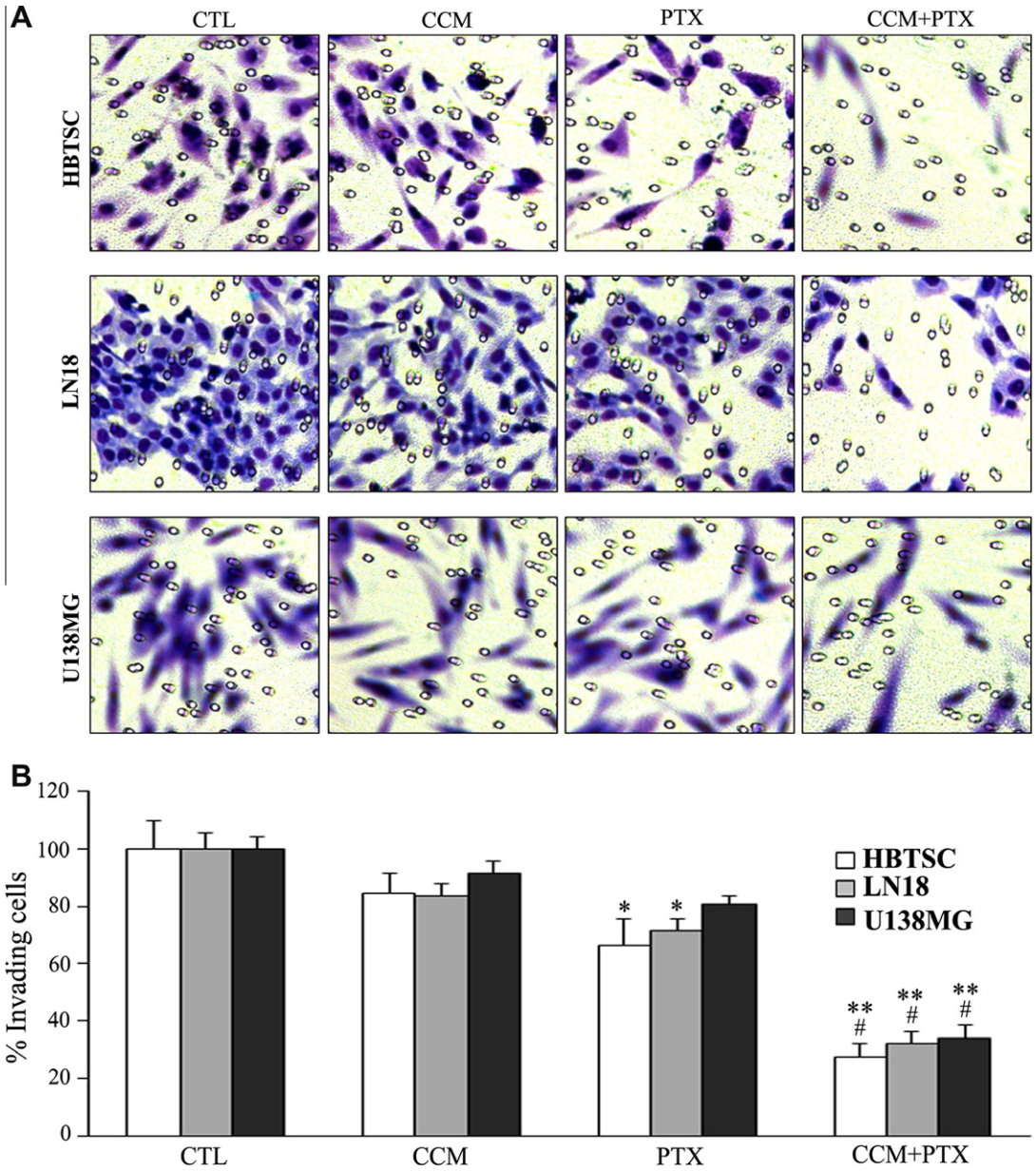

Fig. 6. *In vitro* cell invasion assay. Treatments (24 h): control (CTL), 20 μM CCM, 10 nM PTX, and 20 μM CCM + 10 nM PTX. (A) Matrigel cell invasion assay. (B) Quantitation of matrigel invaded cells. Mean values ($n = 3$) are shown ($^{*}p < 0.05$; $^{**}p < 0.01$; and $^{\#}p < 0.01$ where * or ** compared single treatment with CTL; # compared combination treatment with single treatment).

low doses to inhibit the growth of not only HBTSC but also glioblastoma cells and thereby implied the possibility of elimination of brain tumor altogether.

PTX, which is a widely used as anti-cancer chemotherapy, binds to the β-subunit of tubulin and blocks the microtubule's normal functions and mitosis (McGrogan et al., 2008). However, high dose of PTX may have the cytotoxic effects in normal cell division. In this study we found that a low dose of CCM (20 μM) acted synergistically with a low dose of PTX (10 nM) to induce apoptosis without any necrosis. It is noteworthy that we have achieved significant anti-cancer efficacy with low dose of PTX (10 nM) in our current *in vitro* combination therapy, whereas we have used 10 times more PTX (100 nM) to achieve significant anti-cancer efficacy in a previous combination therapy in animals (George et al., 2009). Use of high dose of PTX in cancer therapy in animals has been associated with severe side effects (Sheihet et al., 2012) and high mortality rates (Vassileva et al., 2007). Adverse events are also most frequently observed in cancer patients after treatment with high dose of PTX (van Herpen et al., 2010). Our current study suggests that use of low dose of PTX (10 nM) in combination therapy provides anti-cancer effects *in vitro* and should be equally effective but less toxic in animals as well as in the clinical setting in patients.

CCM can activate the extrinsic pathway of apoptosis in glioblastoma cells as evidenced from activation of caspase-8 and cleavage of Bid to tBid (Karmakar et al., 2006). Then, tBid translocation to mitochondrial membrane may trigger release of several pro-apoptotic factors including cytochrome *c*, Smac/Diablo, and AIF into the cytosol to facilitate apoptosis (Kim, 2005). We found that combination of CCM and PTX was highly effective in activation of caspase-8 and cleavage of Bid to tBid, mitochondrial release of cytochrome *c*, Smac/Diablo, and AIF into the cytosol in HBTSC, LN18, and U138MG cells, indicating the induction both extrinsic and intrinsic pathways of apoptosis.

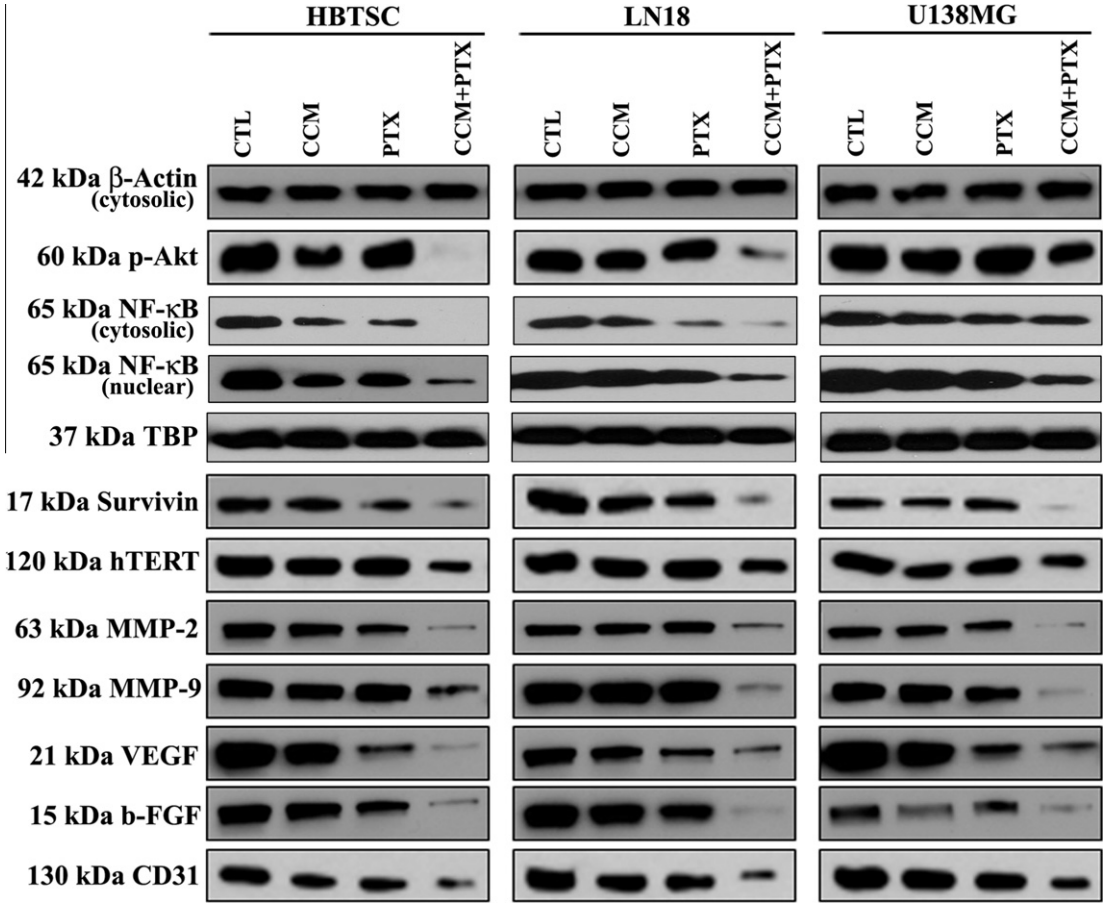

Fig. 7. Western blotting to examine molecules involved in cell survival (p-Akt and NF-κB), proliferation (survivin and hTERT), invasion (MMP-2 and MMP-9), and angiogenesis (VEGF, b-FGF, and CD31) in HBTSC, LN18, and U138MG cells. Treatments (24 h): control (CTL), 20 μM CCM, 10 nM PTX, and 20 μM CCM + 10 nM PTX. All experiments were repeated three times.

Caspase-8 mediated cleavage of Bid to tBid and translocation of tBid to mitochondria provides a link between death receptor and mitochondrial pathways of apoptosis (Fulda and Debatin, 2006). Caspase-8 mediated cleavage of Bid to tBid alters the expression of Bax and Bcl-2 (Choudhury et al., 2011). An increase in Bax:Bcl-2 ratio is a key factor to trigger the release of several pro-apoptotic molecules from mitochondria (Karmakar et al., 2006). Upregulation of various anti-apoptotic molecules such as Bcl-2 protects cancer cells from apoptosis (George et al., 2009). We found that combination of CCM and PTX caused significant upregulation of Bax with concomitant down-regulation of Bcl-2, in essence, leading to an increase in the Bax:Bcl-2 ratio. Various studies demonstrated that phosphorylation caused inactivation of Bcl-2 to favor activation of mitochondrial pathway of apoptosis (Haldar et al., 1995; Pathan et al., 2001). It is now well known that drug affecting microtubule polymerization is capable of inducing the formation of p-Bcl-2 (Haldar et al., 1998; Srivastava et al., 1999). PTX can also induce apoptosis by formation of p-Bcl-2 in glioblastoma cells (Das et al., 2008a). Current study showed that combination of CCM and PTX increased p-Bcl-2, indicating that formation of p-Bcl-2 played an important role in the potentiation of mitochondrial pathway of apoptosis.

Activation of mitochondrial pathway drives activation of the effector caspases including caspase-3 to cleave a number of cytoplasmic and nuclear substrates leading to apoptosis (Karmakar et al., 2006). Calpain and caspase-3 activities are known to be simultaneously activated in human glioblastoma cells (Choudhury et al., 2011) and glioblastoma T98G xenograft (Karmakar et al., 2010). Cytochrome *c* released from mitochondria into cytosol binds to apoptosis-activating-factor-1 (Apaf-1) to produce apoptosome leading to the activation caspase-9 and then caspase-3 for caspase-dependent apoptosis (Kim, 2005). In this study, we demonstrated that CCM in combination with PTX played an important role in dramatic increase in activation of both calpain and caspase-3. Increased activities of calpain and caspase-3 generated 145 kDa SBDP and 120 kDa SBDP, respectively. Also, increased caspase-3 activity mediated ICAD cleavage and PARP fragmentation. Cleavage of ICAD can allow the cells to translocate CAD to the nucleus for nuclear DNA fragmentation, the final event in apoptosis.

Glioblastoma cells are highly invasive and can infiltrate the extracellular matrix of normal tissue, making it highly difficult to treat glioblastoma using surgery and radiation (Giese et al., 2003). It has been previously reported that PTX reduced the cell invasion and migration in human glioblastoma cells (George et al., 2009) and ovarian cancer cells (Westerlund et al., 1997). We performed the *in vitro* matrigel invasion assay and found that combination therapy most drastically reduced cell invasion.

It is known that p-Akt (active form of Akt) promotes cell survival and proliferation via activation of NF-κB pathway (Maddika et al., 2007). Activation of Akt kinase activity stimulates cell survival through upregulation of NF-κB (Pelloski et al., 2006). CCM in combination with PTX effectively reduced expression of p-Akt and NF-κB to promote apoptosis (Bava et al., 2005). We also found that CCM in combination with PTX prominently reduced the

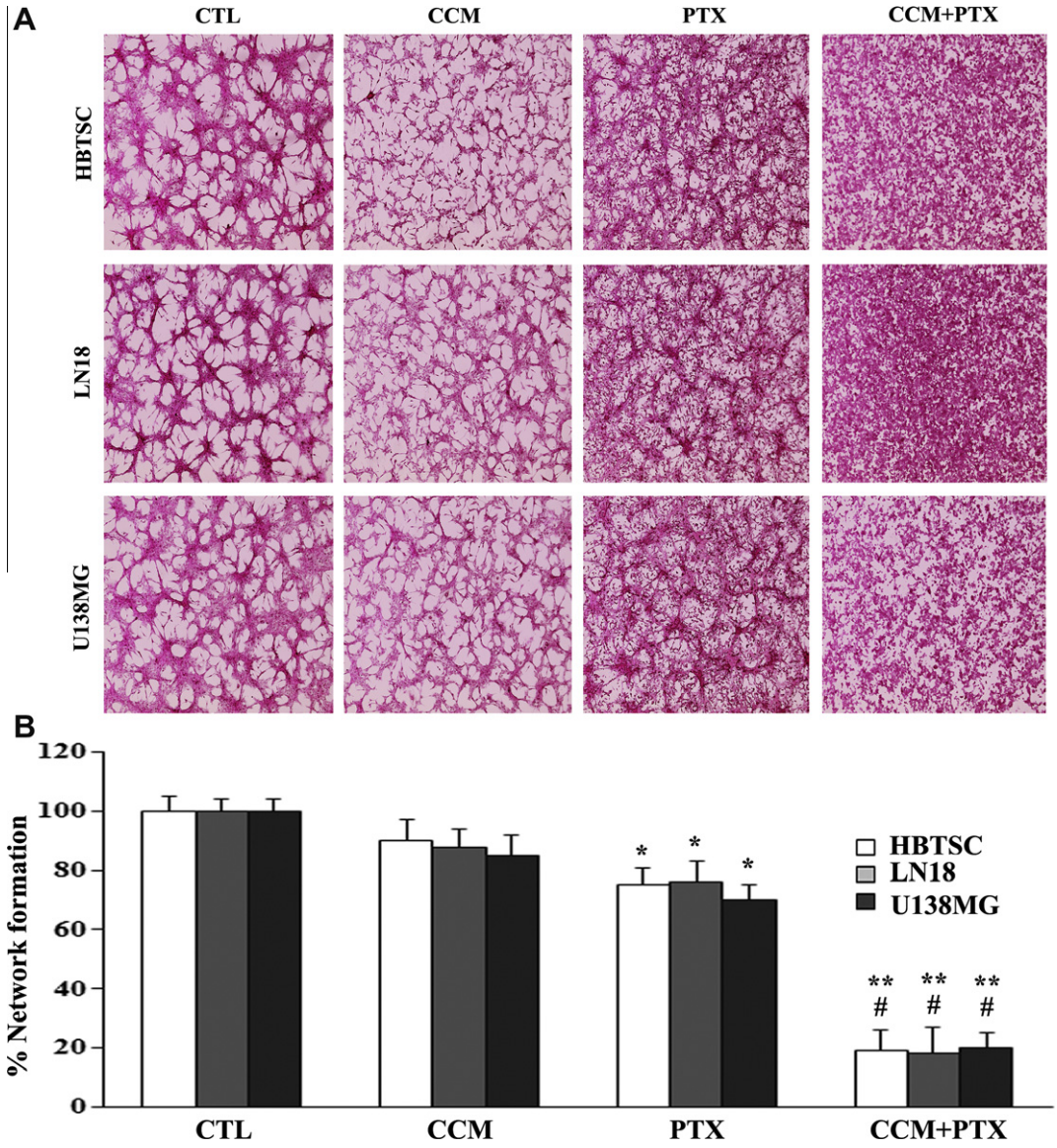

Fig. 8. *In vitro* network formation assay. Treatments (24 h): control (CTL), 20 μM CCM, 10 nM PTX, and 20 μM CCM + 10 nM PTX. (A) *In vitro* network formation in HME cells co-cultured with CTL and treated HBTSC, LN18, or U138MG cells. (B) Quantitation of *in vitro* network formation. Mean values ($n = 3$) are shown ($^{*}p < 0.05$; $^{**}p < 0.01$; and $^{\#}p < 0.01$ where * or ** compared single treatment with CTL; # compared combination treatment with single treatment).

expression of cytosolic and nuclear NF-κB in HBTSC, LN18, and U138MG cells.

Survivin knockdown promoted apoptosis and inhibited cell invasion, angiogenesis, and tumorigenesis in human glioblastoma (George et al., 2010b). Both VEGF and b-FGF are key angiogenic factors and CD31 is a marker for angiogenesis, the formation of new blood vessels. Angiogenesis plays an important role in tumor progression and metastasis. Angiogenesis surrounds the microenvironment due to activation of pro-angiogenic growth factors such as VEGF and b-FGF and also invasive factors such as MMPs (Chesler et al., 2007). hTERT, an enzyme required for telomerase activity, is an important factor in cell proliferation and cell viability (George et al., 2010a). We found that combination of CCM and PTX efficiently down-regulated the molecules involved in cell proliferation (survivin and hTERT), invasive (MMP-2 and MMP-9), and angiogenic (VEGF and b-FGF) pathways and also observed dramatic decreases in the angiogenesis marker CD31 in HBTSC, LN18, and U138MG cells. The *in vitro* network formation requires special angiogenic stimulants such as VEGF and b-FGF secreted by the tumor cells. We found that HBTSC, LN18, and U138MG cells after treatment with combination of CCM and PTX markedly reduced angiogenic factors and capability of network formation.

5. Conclusion

In conclusion, our current investigation clearly showed that combination of CCM and PTX acted synergistically to control the growth of HBTSC, LN18, and U138MG cells by increasing apoptosis via multiple molecular mechanisms leading to activation of proteolytic activities of calpain and caspase-3 and also by inhibiting survival, invasive, and angiogenic signaling pathways.

Acknowledgements

This work was supported in part by the grants from the National Institutes of Health (R01 NS65456) and the South Carolina

Spinal Cord Injury Research Fund (SCIRF-11-002). Authors have no conflict of interest to acknowledge.

References

Bao, S., Wu, Q., McLendon, R.E., Hao, Y., Shi, Q., Hjelmeland, A.B., Dewhirst, M.W., Bigner, D.D., Rich, J.N., 2006. Glioma stem cells promote radioresistance by preferential activation of the DNA damage response. Nature 444, 756–760.

Bava, S.V., Puliappadamba, V.T., Deepti, A., Nair, A., Karunagaran, D., Anto, R.J., 2005. Sensitization of taxol-induced apoptosis by curcumin involves down-regulation of nuclear factor-kappaB and the serine/threonine kinase Akt and is independent of tubulin polymerization. J. Biol. Chem. 280, 6301–6308.

Bleau, A.M., Hambardzumyan, D., Ozawa, T., Fomchenko, E.I., Huse, J.T., Brennan, C.W., Holland, E.C., 2009. PTEN/PI3K/Akt pathway regulates the side population phenotype and ABCG2 activity in glioma tumor stem-like cells. Cell Stem Cell 4, 226–235.

Chesler, L., Goldenberg, D.D., Seales, I.T., Satchi-Fainaro, R., Grimmer, M., Collins, R., Struett, C., Nguyen, K.N., Kim, G., Tihan, T., Bao, Y., Brekken, R.A., Bergers, G., Folkman, J., Weiss, W.A., 2007. Malignant progression and blockade of angiogenesis in a murine transgenic model of neuroblastoma. Cancer Res. 67, 9435–9442.

Choudhury, S.R., Karmakar, S., Banik, N.L., Ray, S.K., 2011. Valproic acid induced differentiation and potentiated efficacy of taxol and nanotaxol for controlling growth of human glioblastoma LN18 and T98G cells. Neurochem. Res. 36, 2292–2305.

Choudhury, S.R., Karmakar, S., Banik, N.L., Ray, S.K., 2010. Synergistic efficacy of sorafenib and genistein in growth inhibition by down regulating angiogenic and survival factors and increasing apoptosis through upregulation of p53 and p21 in malignant neuroblastoma cells having N-Myc amplification or non-amplification. Invest. New Drugs 28, 812–824.

Crown, J., O'Leary, M., 2000. The taxanes: an update. Lancet 355, 1176–1178.

Das, A., Banik, N.L., Ray, S.K., 2008a. Retinoids induced astrocytic differentiation with down regulation of telomerase activity and enhanced sensitivity to taxol for apoptosis in human glioblastoma T98G and U87MG cells. J. Neurooncol. 87, 9–22.

Das, S., Srikanth, M., Kessler, J.A., 2008b. Cancer stem cells and glioma. Nat. Clin. Pract. Neurol. 4, 427–435.

Epstein, J., Sanderson, I.R., MacDonald, T.T., 2010. Curcumin as a therapeutic agent: the evidence from in vitro, animal and human studies. Br. J. Nutr. 103, 1545–1557.

Fulda, S., Debatin, K.-M., 2006. Extrinsic versus intrinsic apoptosis pathways in anticancer chemotherapy. Oncogene 25, 4798–4811.

George, J., Banik, N.L., Ray, S.K., 2009. Combination of taxol and Bcl-2 siRNA induces apoptosis in human glioblastoma cells and inhibits invasion, angiogenesis and tumour growth. J. Cell. Mol. Med. 10, 4205–4218.

George, J., Banik, N.L., Ray, S.K., 2010a. Knockdown of hTERT and concurrent treatment with interferon-gamma inhibited proliferation and invasion of human glioblastoma cell lines. Int. J. Biochem. Cell Biol. 42, 1164–1173.

George, J., Banik, N.L., Ray, S.K., 2010b. Survivin knockdown and concurrent 4-HPR treatment controlled human glioblastoma in vitro and in vivo. Neuro-oncol. 12, 1088–1101.

Giese, A., Bjerkvig, R., Berens, M.E., Westphal, M., 2003. Cost of migration: invasion of malignant gliomas and implications for treatment. J. Clin. Oncol. 21, 1624–1636.

Gilbert, C.A., Ross, A.H., 2009. Cancer stem cells: cell culture, markers and targets for new therapies. J. Cell. Biochem. 108, 1031–1038.

Haldar, S., Basu, A., Croce, C.M., 1998. Serine-70 is one of the critical sites for drug-induced Bcl2 phosphorylation in cancer cells. Cancer Res. 58, 1609–1615.

Haldar, S., Jena, N., Croce, C.M., 1995. Inactivation of Bcl-2 by phosphorylation. Proc. Natl. Acad. Sci. USA 92, 4507–4511.

Huang, E.H., Hynes, M.J., Zhang, T., Ginestier, C., Dontu, G., Appelman, H., Fields, J.Z., Wicha, M.S., Boman, B.M., 2009. Aldehyde dehydrogenase 1 is a marker for normal and malignant human colonic stem cells (SC) and tracks SC overpopulation during colon tumorigenesis. Cancer Res. 69, 3382–3389.

Jiang, F., Qiu, Q., Khanna, A., Todd, N.W., Deepak, J., Xing, L., Wang, H., Liu, Z., Su, Y., Stass, S.A., Katz, R.L., 2009. Aldehyde dehydrogenase 1 is a tumor stem cell-associated marker in lung cancer. Mol. Cancer Res. 7, 330–338.

Karmakar, S., Banik, N.L., Patel, S.J., Ray, S.K., 2006. Curcumin activated both receptor-mediated and mitochondria-mediated proteolytic pathways for apoptosis in human glioblastoma T98G cells. Neurosci. Lett. 407, 53–58.

Karmakar, S., Banik, N.L., Ray, S.K., 2007. Curcumin suppressed anti-apoptotic signals and activated cysteine proteases for apoptosis in human malignant glioblastoma U87MG cells. Neurochem. Res. 32, 2103–2113.

Karmakar, S., Choudhury, S.R., Banik, N.L., Ray, S.K., 2010. Activation of multiple molecular mechanisms for increasing apoptosis in human glioblastoma T98G xenograft. J. Cancer Sci. Ther. 2, 107–113.

Karunagaran, D., Rashmi, R., Kumar, T.R., 2005. Induction of apoptosis by curcumin and its implications for cancer therapy. Curr. Cancer Drug Targets 5, 117–129.

Kim, R., 2005. Recent advances in understanding the cell death pathways activated by anticancer therapy. Cancer 103, 1551–1560.

Maddika, S., Ande, S.R., Panigrahi, S., Paranjothy, T., Weglarczyk, K., Zuse, A., Eshraghi, M., Manda, K.D., Wiechec, E., Los, M., 2007. Cell survival, cell death and cell cycle pathways are interconnected: implications for cancer therapy. Drug Resist. Updates 10, 13–29.

McGrogan, B.T., Gilmartin, B., Carney, D.N., McCann, A., 2008. Taxanes, microtubules and chemoresistant breast cancer. Biochim. Biophys. Acta 1785, 96–132.

Pathan, N., Aime-Sempe, C., Kitada, S., Haldar, S., Reed, J.C., 2001. Microtubule-targeting drugs induce Bcl-2 phosphorylation and association with Pin1. Neoplasia 3, 70–79.

Pelloski, C.E., Lin, E., Zhang, L., Yung, W.K., Colman, H., Liu, J.L., Woo, S.Y., Heimberger, A.B., Suki, D., Prados, M., Chang, S., Barker 3rd, F.G., Fuller, G.N., Aldape, K.D., 2006. Prognostic associations of activated mitogen-activated protein kinase and Akt pathways in glioblastoma. Clin. Cancer Res. 12, 3935–3941.

Porter, K.R., McCarthy, B.J., Freels, S., Freels, S., Kim, Y., Davis, F.G., 2010. Prevalence estimates for primary brain tumors in the United States by age, gender, behavior, and histology. Neuro-oncol. 12, 520–527.

Purnanam, K.L., Boustany, R.M., 1999. Assessment of cell viability and histochemical methods in apoptosis. In: Hannun, Y.A., Boustany, R.M. (Eds.), Apoptosis in Neurobiology. CRC, New York, pp. 129–152.

Rasper, M., Schafer, A., Piontek, G., Teufel, J., Brockhoff, G., Ringel, F., Heindl, S., Zimmer, C., Schlegel, J., 2010. Aldehyde dehydrogenase 1 positive glioblastoma cells show brain tumor stem cell capacity. Neuro-oncol. 12, 1024–1033.

Reya, T., Morrison, S.J., Clarke, M.F., Weissman, I.L., 2001. Stem cells, cancer, and cancer stem cells. Nature 414, 105–111.

Rowinsky, E.K., Wright, M., Monsarrat, B., Lesser, G.J., Donehower, R.C., 1993. Taxol: pharmacology, metabolism and clinical implications. Cancer Surv. 17, 283–2304.

Sell, S., 2006. Potential gene therapy strategies for cancer stem cells. Curr. Gene Ther. 6, 579–591.

Sheihet, L., Garbuzenko, O.B., Bushman, J., Gounder, M.K., Minko, T., Kohn, J., 2012. Paclitaxel in tyrosine-derived nanospheres as a potential anti-cancer agent: in vivo evaluation of toxicity and efficacy in comparison with paclitaxel in Cremophor. Eur. J. Pharm. Sci. 45, 320–329.

Shi, C.J., Gao, J., Wang, M., Wang, X., Tian, R., Zhu, F., Shen, M., Qin, R.Y., 2011. $CD133^{+}$ gallbladder carcinoma cells exhibit self-renewal ability and tumorigenicity. World J. Gastroenterol. 17, 2965–2971.

Srivastava, R.K., Mi, Q.S., Hardwick, J.M., Longo, D.L., 1999. Deletion of the loop region of Bcl-2 completely blocks paclitaxel-induced apoptosis. Proc. Natl. Acad. Sci. USA 96, 3775–3780.

Stearns, M.E., Wang, M., 1992. Taxol blocks processes essential for prostate tumor cell (PC-3 ML) invasion and metastases. Cancer Res. 52, 3776–3781.

Toiyama, Y., Inoue, Y., Hiro, J., Ojima, E., Watanabe, H., Narita, Y., Okigami, M., Hosono, A., Miki, C., Kusunoki, M., 2009. Paclitaxel inhibits radiation induced VEGF secretion and enhances radiosensitizing effects in human colon cancer cell HT29. Cancer Ther. 7, 123–132.

van Herpen, C.M., Eskens, F.A., de Jonge, M., Desar, I., Hooftman, L., Bone, E.A., Timmer-Bonte, J.N., Verweij, J., 2010. A Phase Ib dose-escalation study to evaluate safety and tolerability of the addition of the aminopeptidase inhibitor tosedostat (CHR-2797) to paclitaxel in patients with advanced solid tumours. Br. J. Cancer 103, 1362–1368.

Vassileva, V., Grant, J., De Souza, R., Allen, C., Piquette-Miller, M., 2007. Novel biocompatible intraperitoneal drug delivery system increases tolerability and therapeutic efficacy of paclitaxel in a human ovarian cancer xenograft model. Cancer Chemother. Pharmacol. 60, 907–914.

Westerlund, A., Hujanen, E., Höyhtyä, M., Puistola, U., Turpeenniemi-Hujanen, T., 1997. Ovarian cancer cell invasion is inhibited by paclitaxel. Clin. Exp. Metast. 3, 318–328.

Xiao, H., Verdier-Pinard, P., Fernandez-Fuentes, N., Burd, B., Angeletti, R., Fiser, A., Horwitz, S.B., Orr, G.A., 2006. Insights into the mechanism of microtubule stabilization by taxol. Proc. Natl. Acad. Sci. USA 103, 10166–10173.

Zhou, B.B., Zhang, H., Damelin, M., Geles, K.G., Grindley, J.C., Dirks, P.B., 2009. Tumour-initiating cells: challenges and opportunities for anticancer drug discovery. Nat. Rev. Drug Discov. 8, 806–823.